PAPER • OPEN ACCESS

Magnetically induced anisotropy of flux penetration into strong-pinning superconductor/ferromagnet bilayers

PAPER

Magnetically induced anisotropy of flux penetration into strong-pinning superconductor/ferromagnet bilayers

J Simmendinger[1,6], J Hänisch[2] , M Bihler[1], A M Ionescu[1], M Weigand[1], M Sieger[3], R Hühne[3] , H Rijckaert[4] , I van Driessche[4] , G Schütz[1] and J Albrecht[5]

1 Max-Planck-Institute for Intelligent Systems, Heisenbergstr. 3, D-70569 Stuttgart, Germany
2 Karlsruhe Institute of Technology, Institute for Technical Physics (ITEP), Hermann-von-Helmholtz-Platz 1, D-76344 Eggenstein-Leopoldshafen, Germany
3 Leibniz Institute for Solid State and Materials Research IFW Dresden, Institute for Metallic Materials, Helmholtzstr. 20, D-01069 Dresden, Germany
4 Ghent University, SCRiPTS, Department of Chemistry, Krijgslaan 281-S3, B-9000 Ghent, Belgium
5 Research Institute for Innovative Surfaces FINO, Aalen University, Beethovenstr. 1, D-73430 Aalen, Germany
6 Author to whom any correspondence should be addressed.
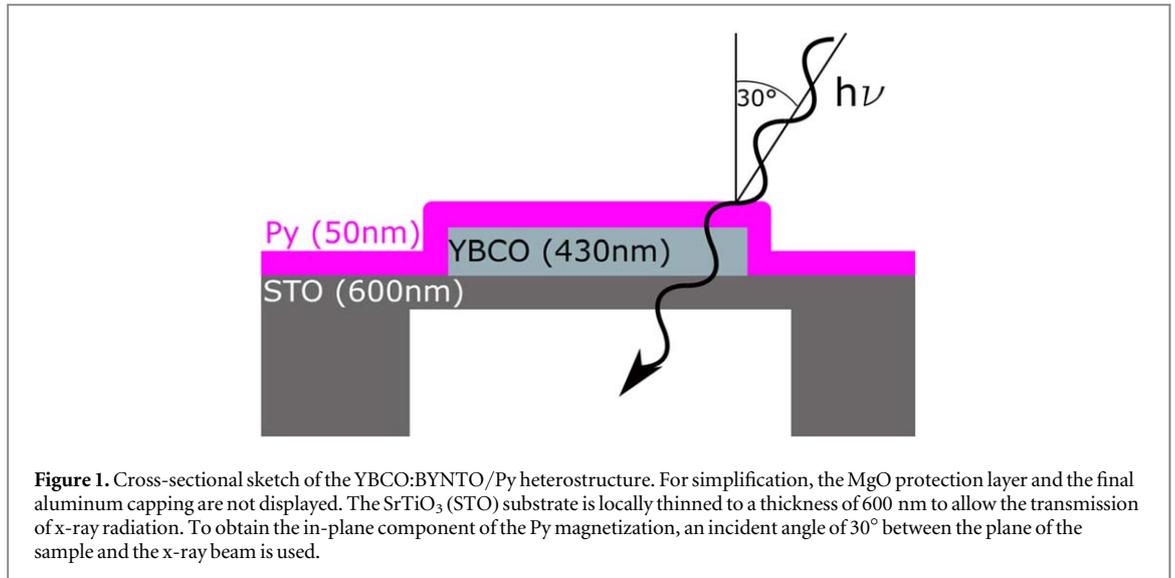
E-mail: simmendinger@is.mpg.de

Abstract

We studied the impact of soft ferromagnetic permalloy (Py) on the shielding currents in a strong-pinning superconductor—$YBa_2Cu_3O_{7-\delta}$ with $Ba_2Y(Nb/Ta)O_6$ nano-precipitates—by means of scanning transmission x-ray microscopy. Typically and in particular when in the thin film limit, superconductor/ferromagnet (SC/FM) bilayers exhibit isotropic properties of the flux line ensemble at all temperatures. However, in elements with small aspect ratio a significant anisotropy in flux penetration is observed. We explain this effect by local in-plane fields arising from anisotropic magnetic stray fields originated by the ferromagnet. This leads to direction-dependent motion of magnetic vortices inside the SC/FM bilayer. Our results demonstrate that small variations of the magnetic properties can have huge impact on the superconductor.

The interaction between superconductors and ferromagnets is complex. Most prominent is the well-studied proximity effect, which occurs at interfaces between superconductor (SC) and ferromagnet (FM). It describes the penetration of superconducting correlations into the ferromagnet and of non-superconducting quasiparticles into the superconductor [1, 2]. Since the transparency of the interface plays a crucial role, the proximity effect can be switched off by introducing an insulating layer between SC and FM [3]. As a result, the interaction across the interface is basically limited to magnetic dipole coupling. In millimeter-sized elements the impact of the ferromagnetic stray field on the magnetic screening of the superconductor is rather small. However, it becomes a key factor in elements with reduced lateral sample size w towards the micrometer-regime while the thickness is kept constant [4–7]. Here, the local field direction is modified by the magnetic spin order in the ferromagnet. This leads to unique properties in micron-sized SC/FM heterostructures whereby they become promising candidates for applications in the field of spintronics [8, 9] as well as for electronic devices [10, 11].

In this paper we study the change of local flux penetration into $YBa_2Cu_3O_{7-\delta}$–$Ba_2Y(Nb/Ta)O_6$ nanocomposite (YBCO:BYNTO) thin films by an adjacent soft-ferromagnetic permalloy (Py, $Ni_{0.8}Fe_{0.2}$) layer. Owing to the large interface roughness of the YBCO:BYNTO thin film a finite demagnetization factor in the plane of the Py is introduced. This is characteristic for high-temperature superconductors and a key difference to recent studies on related SC/FM systems [10, 12]. We used the x-ray microscope MAXYMUS at Bessy II in Berlin to visualize the flux penetration into small superconducting elements. The method of magnetic scanning transmission x-ray microscopy (MSTXM) enables such measurements in a broad range of temperature and magnetic field. MSTXM at low temperatures has been proven to be a powerful tool to investigate micron sized SC/FM elements. The combination of a structural and spatial magnetic resolution of less than 30 nm [13] and

Figure 1. Cross-sectional sketch of the YBCO:BYNTO/Py heterostructure. For simplification, the MgO protection layer and the final aluminum capping are not displayed. The SrTiO$_3$ (STO) substrate is locally thinned to a thickness of 600 nm to allow the transmission of x-ray radiation. To obtain the in-plane component of the Py magnetization, an incident angle of 30° between the plane of the sample and the x-ray beam is used.

100 nm [14], respectively, qualifies MSTXM most for our purpose. The unique setup includes a liquid-helium cryostat with a base temperature of $T_{base} = 20$ K and a magnetic system to apply fields up to $B_{ext} = 40$ mT.

Magneto-optical imaging (MOFE) technique is used to support the size-dependent analysis of the bilayers by characterizing elements with $w \geqslant 100$ μm. Here, ferromagnetic iron garnet films are used to depict the local magnetic field density distribution with a spatial resolution of about 5 μm [15] . We refer to the review article of Jooss *et al* [5] for a detailed description of the method.

Py serves at the same time as sensing layer for the chosen microscopy method. The ferromagnet allows the exploitation of the x-ray magnetic circular dichroism (XMCD) effect for nanoscopic imaging. We use ion beam sputtering at room temperature to deposit Py directly on top of the superconductor. Here, its small and temperature-independent coercive field [14] is ideal to depict the local magnetic stray field of the SC/FM bilayer [14, 16, 17]. A protection layer of 10 nm MgO is furthermore deposited between superconductor and ferromagnet to reduce pair-breaking effects. As previously reported, the interaction across the interface is dominated by magnetic dipolar coupling [18–20].

Transmission measurements require an overall sample thickness of less than one micron, due to large absorption coefficients in the soft x-ray regime. Since YBCO:BYNTO thin films can only be grown in reasonable quality on matching single-crystalline substrates, the substrate thickness has to be reduced after the growth process by mechanical cutting and focused ion-beam (FIB) milling [21] to below 600 nm. A sketch of the typical sample geometry is shown in figure 1.

The superconductor used in this work is a ~430 nm thick YBCO film with insulating BYNTO nanocolumnar inclusions as confirmed via a TEM cross-sectional image (*vide infra*). YBCO is a ceramic type-II superconductor with a critical temperature of about 90 K and an extraordinarily high upper critical field that makes it very attractive for a manifold of applications from the power sector to high-energy physics [22]. The irreversibility field, i.e. the magnetic field up to which vortices are pinned effectively and loss-free current transport is possible, can be enlarged by the introduction of secondary phases (e.g. BYNTO) to the YBCO matrix and other methods [23]. The film has been prepared on a 5 × 5 mm^2 single-crystalline (100)-oriented SrTiO$_3$ (STO) substrate by pulsed laser deposition from a mixed target of 95 mol% YBCO and 5 mol% BYNTO, as described by Opherden *et al* [23] and Sieger *et al* [24]. Subsequent oxygen annealing leads to optimal doping and a T_c of about 90 K.

Artificial defects with dimensions in the range of a few nanometers are very effective pinning centers. The mixed double-perovskite BYNTO has several advantages compared to the up-to-now commonly used single-perovskites BaMO$_3$ (M transition metal) including the easy self-assembly of cube-on-cube aligned, highly correlated nanosized columns (figure 2) being able to trap magnetic flux aligned in their main direction [25, 26].

Intense research is devoted to pinning engineering, i.e. creating nanostructures with adapted size, orientation and distributions to achieve very high pinning forces, e.g. 25 GN m^{-3} (77 K, 2.3 T) for a similar YBCO:BYNTO film, which is among the highest values reported for YBCO nanocomposite films [25]. For the transmission electron microscope (TEM) analysis, a cross-sectional lamella has been obtained using ion milling techniques via the FIB *in situ* lift-out procedure with an Omniprobe extraction needle and top cleaning.

The cross-sectional bright field-TEM image (figure 2) shows the fully biaxial (00ℓ) texture of the YBCO: BYNTO layer with cube-on-cube orientation relationship between the YBCO:BYNTO layer and the STO substrate. It contains straight BYNTO nanocolumns which are flexural and splayed around 3° and Y$_2$O$_3$
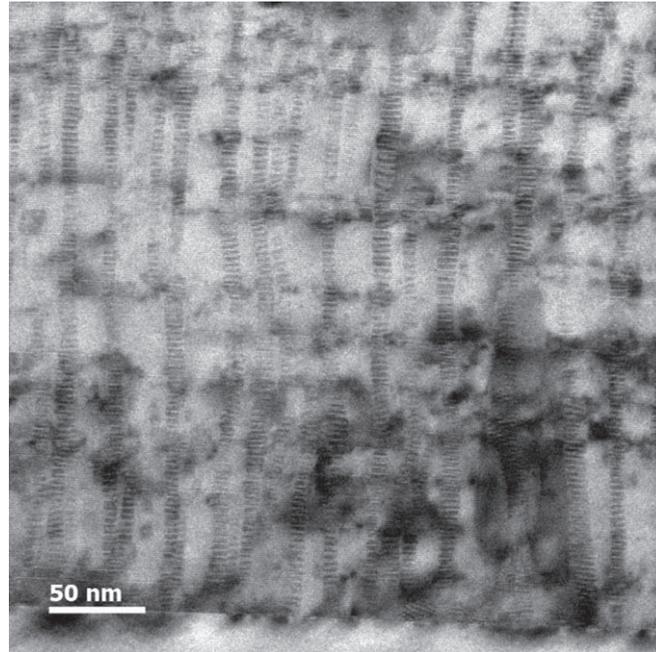
Figure 2. Bright-field transmission electron microscope image of the YBCO:BYNTO film close to the interface of the STO single-crystal. BYNTO-nanocolumns with a diameter of about 7.5 nm (vertical) and Y_2O_3 platelets (horizontal) as well as occasional *ab*-aligned stacking faults are present.
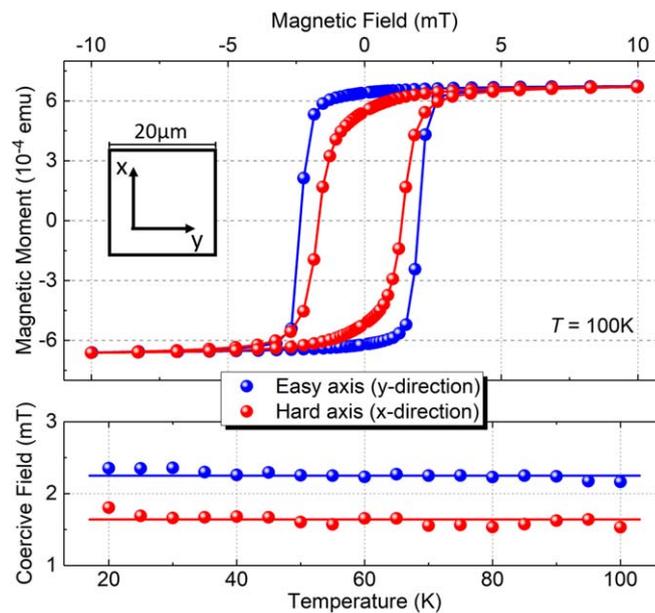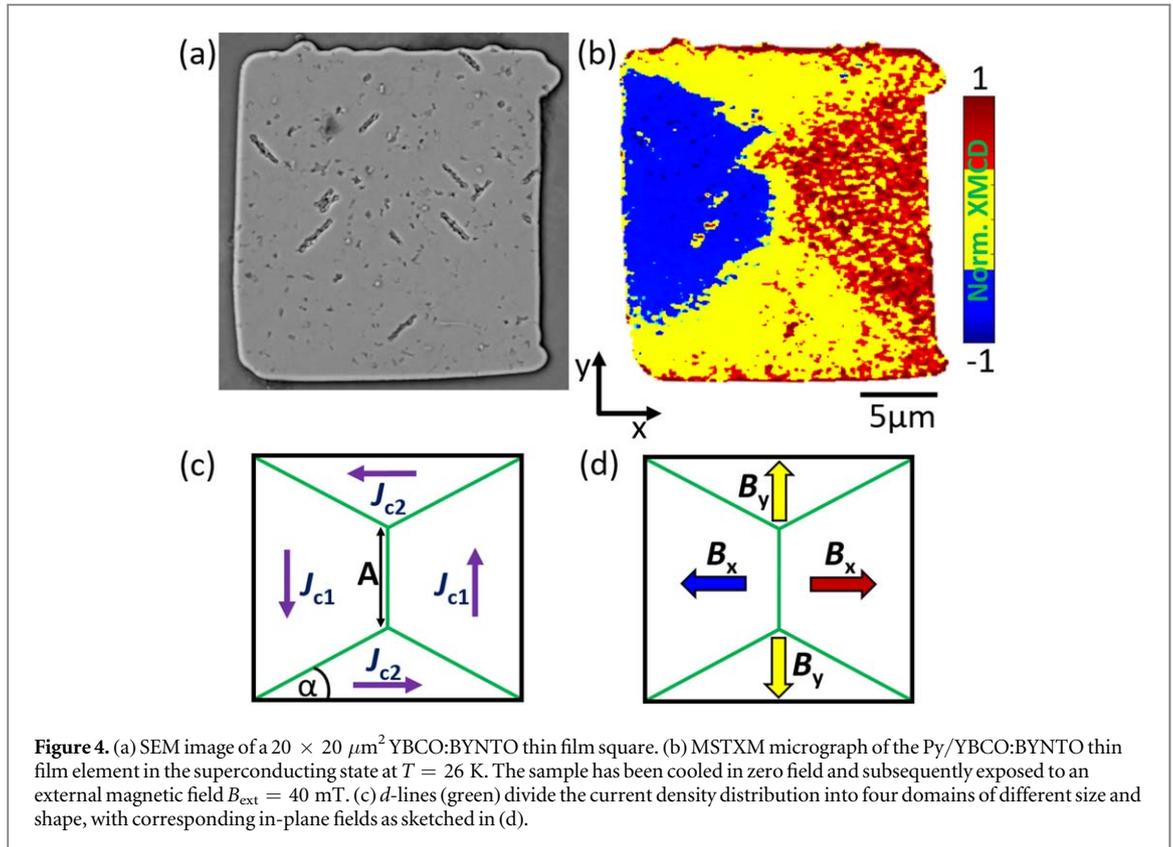

Figure 3. (Top) SQUID hysteresis loops in the plane (*x*- and *y*-direction) of 50 nm Py on YBCO measured at $T = 100$ K. (Bottom) The difference between the coercive field B_c in *x*- and *y*-direction is larger than 0.5 mT in the temperature range from 20 to 100 K.

platelets. The density of these BYNTO nanocolumns in YBCO is 1 nanocolumn per 39 nm. The diameter of nanocolumns is 7.6 ± 1.4 nm with spacing of 16.3 ± 3.6 nm. Also *ab*-aligned stacking faults can be observed between the nanocolumns.

The prepared bilayered samples are first characterized by SQUID magnetometry at temperatures above the superconducting transition. The magnetic response of the ferromagnetic layer for varying in-plane fields $B_{\text{ext},\parallel}$ is exemplified at $T = 100$ K in figure 3. There is a smooth change along the hard axis (*x*-direction) with a coercive field of about 1.6 mT, whereas a square-shaped loop with enlarged coercive field of about 2.2 mT is observed along the easy axis (*y*-direction) [27]. The coercive fields are nearly independent of temperature in the relevant range from 20 to 100 K, as depicted in the bottom panel of figure 3.

Figure 4. (a) SEM image of a $20 \times 20\ \mu m^2$ YBCO:BYNTO thin film square. (b) MSTXM micrograph of the Py/YBCO:BYNTO thin film element in the superconducting state at $T = 26$ K. The sample has been cooled in zero field and subsequently exposed to an external magnetic field $B_{ext} = 40$ mT. (c) *d*-lines (green) divide the current density distribution into four domains of different size and shape, with corresponding in-plane fields as sketched in (d).

We investigated the impact of the in-plane anisotropic ferromagnet onto the superconductor by means of MSTXM to locally depict the magnetic flux distribution inside the YBCO thin film. Therefore, a $20 \times 20\ \mu m^2$ SC/FM element is cooled to a temperature $T = 26$ K in zero-field. Subsequently, an external out-of-plane field $B_{ext,\perp} = 40$ mT is applied to force magnetic flux to penetrate the superconductor. As depicted in figure 4(b), the superconductor is now in the critical state with supercurrents flowing throughout the whole film. This leads to a roof-shaped geometry with discontinuity-lines (*d*-lines) separating domains where the supercurrents sharply bend by 90° to adjust to the shape of the sample, as sketched in figure 4(c). The corresponding in-plane field components are the measured signal (see figure 4(d)), introducing a multicolored state. The MSTXM method is only sensitive to the magnetization of the Py in *x*-direction being parallel to the incident vector of the *x*-ray beam. Thus, the normalized XMCD signal solely exhibits finite values in the left and right domain.

In isotropic quadratic films, *d*-lines meet in the center of the square, whereby $\alpha = 45°$ and the anisotropy ratio $A_J = J_{c1}/J_{c2} = 1/\tan(\alpha)$ equals unity. This is obviously not the case for small Py/YBCO:BYNTO thin film elements, as can be seen in figures 4(b)–(d). We find enlarged blue/red domains in comparison to the yellow domains. Magnetic flux penetrates faster into the left and right part of the film compared to the top and bottom part. To understand why the domains are not of equal size, we first analyzed the influence of the sample preparation on the superconducting anisotropic properties. Here, the prime suspect is ion-beam milling with Ga^+-ions that might introduce a structural anisotropy into the SC/FM films. Therefore, two MSTXM measurements were performed at the same element. In between these measurements the STO substrate was thinned starting from 600 to 400 nm. The perfect agreement between the resulting anisotropy ratios of $A_j(26\ K) \sim 1.27$ (see red triangle and green circle in figure 5) excludes effects stemming from possible implementation of Ga^+-Ions into the superconductor.

The anisotropy ratios A_j of two different $20 \times 20\ \mu m^2$ squares are plotted as function of temperature in figure 5. The processing method for each image involves a line-wise tangent-fit to find the corresponding flux front points followed by a linear fitting approach to extract α. Both elements exhibit a corresponding behavior: up to 50 K $A_j(T)$ is approximately independent of temperature featuring values of $A_j(\text{square 2}) \sim 1.37$ and $A_j(\text{square 1}) \sim 1.27$, respectively.

Similar results were previously reported for superconducting thin films such as MgB_2 [28] and YBCO grown on vicinal-cut STO [29]. For the latter, the authors explained the anisotropy by nanometer-sized pinning centers, so called anti-phase boundaries, with a well-defined ordering. The resulting anisotropic current flow is unaffected by the *w* and A_j strongly increases with reduced temperature. These are the fundamental differences between structurally and magnetically induced anisotropy: Owing to their weak binding potential, atomic
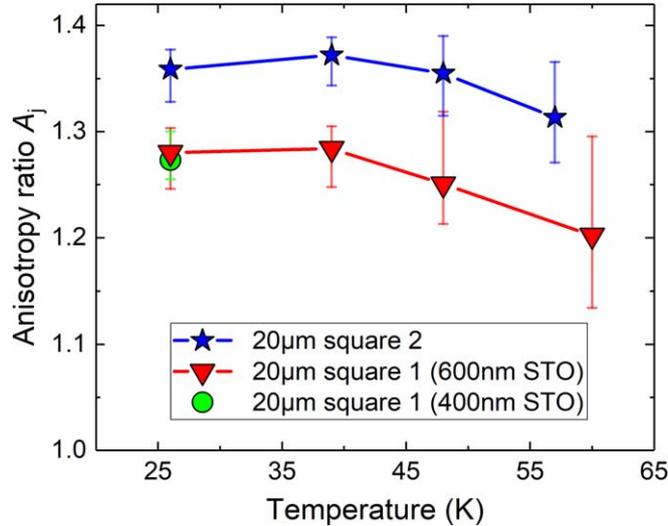
Figure 5. Temperature dependence of the anisotropy ratio A_j for two different squares with 20 μm lateral size. Both samples exhibit the same temperature dependence with comparable absolute values for A_j. For temperatures up to ~50 K, A_j is a nearly temperature independent exhibiting values of ~1.37 (blue stars, square 2) and ~1.27 (red triangles, square 1), respectively. Further increasing the temperature towards 60 K slightly reduces the anisotropy.
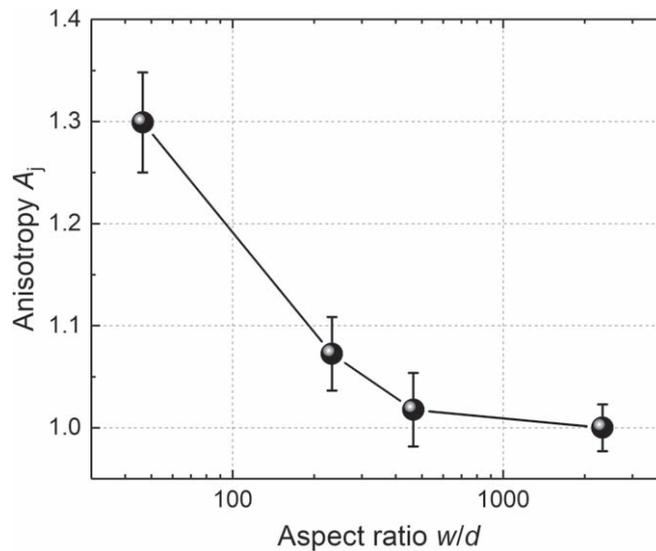

Figure 6. Average anisotropy ratio A_j measured for various aspect ratios at $T = 26$ K. A_j decreases with increasing aspect ratio to eventually approach unity in macroscopic elements with $w/d > 1000$.

defects only pin vortices at low temperatures. With increasing thermal energy the probability of magnetic flux lines being pinned at nanoscopic pinning centers is reduced. Thus, in case of structurally induced anisotropic pinning, $A_j(T)$ should exhibit a strong decrease with increasing temperature as observed in [28, 29], which is not consistent with the results shown in figure 5.

The impact of the aspect ratio w/d onto A_j is shown in figure 6. Here, small elements (20 μm) were analyzed by MSTXM, whereas MOFE microscopy was used for larger elements with w up to 1 mm. The presented data are average values collected from various samples. It becomes apparent that the anisotropy ratio is reduced with increasing w to approach unity in elements of macroscopic size ($w \geqslant 1$ mm). The position of the flux front in small SC/FM elements is strongly influenced by their aspect ratio. The superconducting film provides a magnetic stray field with a complex three-dimensional geometry. In the critical state, at the surface of the YBCO: BYNTO film, the in-plane component of the stray field is constant and proportional to the sheet current. On the other hand, the out-of-plane component was shown to exhibit an increase with the lateral size of the film [6]. This behavior makes the small superconducting elements with efficient flux line pinning to show the largest deviations from the out-of-plane orientation of the local magnetic field. Therefore, the local magnetic field

exhibits a strong inclination, which leads to a change in the flux penetration into small elements compared to mm-sized ones. The soft-magnetic layer on top of the superconductor amplifies the in-plane magnetic components generated by the electric currents in the superconducting thin film.

For an in-plane anisotropic ferromagnetic layer (see figure 3) the resulting local tilt of the magnetic field is also anisotropic. When the in-plane component of the superconductor stray field points along the x-direction (smaller coercive field than in the y-direction), the permalloy reacts faster at the field change and the magnetic field in this direction is enhanced. This leads to a faster flux penetration in the left/right domain in comparison to the top/bottom domain.

Pinning induced anisotropies are supposed to be independent of the aspect ratio, whereby the assumption of magnetically induced current density anisotropies in Py/YBCO:BYNTO bilayers is underpinned.

In conclusion, flux penetration in SC/FM elements can be anisotropic if the involved ferromagnet exhibits anisotropic properties. The observed effect significantly depends on the aspect ratio of the sample. In this work we investigated bilayers consisting of YBCO with BYNTO nanocolumns capped with a ferromagnetic Py layer. We used MSTXM and MOFE microscopy for magnetic analysis with high spatial resolution. In micro-sized elements, the flux distribution in the superconductor exhibits an anisotropic behavior featuring anisotropy ratios of up to 30%. This effect decreases with increasing aspect ratio to finally vanish in the thin film limit. We explain this behavior by both—a locally oblique magnetic field and anisotropic in-plane magnetic properties of the ferromagnetic layer. The ratio between in-plane and out-of-plane field components of a type-II superconductor in the critical state is enlarged with reduced aspect ratio. This effect is amplified by the dipolar-coupling between superconductor stray field and ferromagnetic layer. In addition, the anisotropic in-plane properties of the ferromagnet break the symmetry of the system. Consequently, the penetration of magnetic flux as well as the critical current flow becomes asymmetric in the xy-plane. Our findings are of high importance for any application of SC/FM micro-elements.

ORCID iDs

J Hänisch ⓘ https://orcid.org/0000-0003-2757-236X
R Hühne ⓘ https://orcid.org/0000-0002-0030-6048
H Rijckaert ⓘ https://orcid.org/0000-0002-6078-2919
I van Driessche ⓘ https://orcid.org/0000-0001-5253-3325

References

[1] Soltan S, Albrecht J and Habermeier H U 2004 *Phys. Rev.* B **70** 144517
[2] Sefrioui Z, Arias D, Peña V, Villegas J E, Varela M, Prieto P, León C, Martinez J L and Santamaria J 2003 *Phys. Rev.* B **67** 214511
[3] Albrecht J, Soltan S and Habermeier H U 2005 *Phys. Rev.* B **72** 092502
[4] Brandt E H 1996 *Phys. Rev.* B **54** 4246
[5] Jooss C, Albrecht J, Kuhn H, Leonhardt S and Kronmüller H 2002 *Rep. Prog. Phys.* **65** 651
[6] Brandt E H and Indenbom M 1993 *Phys. Rev.* B **48** 12893
[7] Brandt E H 1998 *Phys. Rev.* B **58** 6506
[8] Eschrig M 2015 *Rep. Prog. Phys.* **78** 104501
[9] Linder J and Robinson J W A 2015 *Nat. Phys.* **11** 307
[10] Vlasko-Vlasov V K, Colauto F, Benseman T, Rosenmann D and Kwok W K 2016 *Sci. Rep.* **6** 36847
[11] Lange M, Van Bael M J, Bruynseraede Y and Moshchalkov V V 2003 *Phys. Rev. Lett.* **90** 197006
[12] Stolyarov V S, Cren T, Brun C, Golovchanskiy I A, Skryabina O V, Kasatonov D I, Khapaev M M, Kupriyanov M Y, Golubov A A and Roditchev D 2018 *Nat. Commun.* **9** 2277
[13] Keskinbora K, Grévent C, Eigenthaler U, Weigand M and Schütz G 2013 *ACS Nano* **7** 9788
[14] Simmendinger J, Ruoss S, Stahl C, Weigand M, Gräfe J, Schütz G and Albrecht J 2018 *Phys. Rev.* B **97** 134515
[15] Dorosinskii L A, Indenbom M V, Nikitenko V I, Ossip'yan Y A, Polyanskii A A and Vlasko-Vlasov V K 1992 *Physica* C **203** 149
[16] Atkinson D, Allwood D A, Xiong G, Cooke M D, Faulkner C C and Cowburn R P 2003 *Nat. Mater.* **2** 85
[17] Trunk T, Redjdal M, Kákay A, Ruane M F and Humphrey F B 2001 *J. Appl. Phys.* **89** 7606
[18] Brisbois J *et al* 2016 *Sci. Rep.* **6** 27159
[19] Hals K M D, Schecter M and Rudner M S 2016 *Phys. Rev. Lett.* **117** 017001
[20] Moshchalkov V V, Golubović D S and Morelle M 2006 *C. R. Phys.* **7** 86
[21] Mayer J, Giannuzzi L A, Kamino T and Michael J 2007 *MRS Bull.* **32** 400
[22] Larbalestier D, Gurevich A, Feldmann D M and Polyanskii A 2001 *Nature* **414** 368
[23] Opherden L *et al* 2016 *Sci. Rep.* **6** 21188
[24] Sieger M *et al* 2017 *IEEE Trans. Appl. Supercond.* **27** 6601407
[25] Ercolano G, Bianchetti M, Wimbush S C, Harrington S A, Wang H, Lee J H and MacManus-Driscoll J L 2011 *Supercond. Sci. Technol.* **24** 095012
[26] Macmanus-Driscoll J L, Foltyn S R, Jia Q X, Wang H, Serquis A, Civale L, Maiorov B, Hawley M E, Maley M P and Peterson D E 2004 *Nat. Mater.* **3** 439

[27] Ben Y J, Vukadinovic N, Billet D and Labrune M 2004 *Phys. Rev. B* **69** 174402
[28] Albrecht J, Matveev A T, Strempfer J, Habermeier H U, Shantsev D V, Galperin Y M and Johansen T H 2007 *Phys. Rev. Lett.* **98** 117001
[29] Jooss C, Warthmann R and Kronmüller H 2000 *Phys. Rev. B* **61** 12433